

Cite this: *J. Mater. Chem. C*,  
2026, 14, 6692

# Synthesis and chiral optical activity of a quadruple heterohelicene based on 1,4-dihydropyrrolo[3,2-*b*]pyrrole–picene hybrid

Krzysztof J. Kochanowski,<sup>af</sup> Krzysztof Górski,<sup>a</sup> Damian Kusy,<sup>a</sup>  
Nicolas Vanthuyne,<sup>b</sup> Alessandro Landi,<sup>c</sup> Francesco Bertocchi,<sup>d</sup>  
Arkadiusz Ciesielski,<sup>e</sup> Michał K. Cyrański,<sup>\*e</sup> Guglielmo Monaco,<sup>\*c</sup>  
Francesca Terenziani<sup>\*d</sup> and Daniel T. Gryko<sup>\*a</sup>

The synthesis and structural elucidation of a diaza-quadruple helicene, comprising a double [6]helicene and two [5]helicene subunits fused around a 1,4-dihydropyrrolo[3,2-*b*]pyrrole (DHPP) core with appended picene units, is reported. The target compound was accessed via a straightforward protocol involving a multicomponent reaction to form a tetraarylpyrrolo[3,2-*b*]pyrrole (TAPP) intermediate, followed by regioselective bromination and a twofold intramolecular direct arylation. X-ray crystallography confirmed the highly twisted, quadruple helical architecture, while separation of the enantiomers of the double anti-*S*<sub>2</sub>-[6]helicene fragment by chiral HPLC enabled comprehensive chiroptical analysis via electronic circular dichroism (ECD) and circularly polarized luminescence (CPL) spectroscopy. Density functional theory (DFT) calculations support the experimental findings by revealing pronounced  $\pi$ -expansion, a distinct charge-transfer character in the excited state, and enhanced alignment of electric and magnetic transition dipole moments, and allow assigning a PP helicity to the central helicenes for the enantiomer whose ECD spectrum has a negative Cotton effect at low energy. Consequently, the structural and chiroptical properties of the diaza-quadruple helicene are thoroughly characterized.

Received 30th December 2025,  
Accepted 22nd February 2026

DOI: 10.1039/d5tc04545b

rsc.li/materials-c

## Introduction

Helicenes represent a remarkable class of screw-shaped, inherently chiral polycyclic aromatic hydrocarbons (PAHs), characterized by a three-dimensional helical structure enforced by steric congestion from *ortho*-fused aromatic rings.<sup>1</sup> This architecture induces chirality without the presence of stereogenic centers, giving rise to pronounced chiroptical properties such as circular dichroism (CD)<sup>2</sup> and circularly polarized luminescence (CPL).<sup>3–5</sup> Since the first report of the parent<sup>5</sup>-azahelicene – the earliest isolated heterohelicene – the chemistry and properties of these

molecules have fascinated researchers for over a century.<sup>6</sup> Their unique structure and exceptional optical and electronic behavior render helicenes highly attractive for a wide spectrum of applications, including (chir)optoelectronics,<sup>7–11</sup> chiral sensing,<sup>12</sup> asymmetric catalysis,<sup>13</sup> and optical data storage.<sup>14</sup>

Advancements in synthetic methodologies have significantly accelerated progress in this field, particularly in the development of heterohelicenes. These approaches have enabled the precise introduction of various heteroatoms – such as nitrogen,<sup>15–23</sup> boron,<sup>24–30</sup> oxygen,<sup>31</sup> sulfur,<sup>32,33</sup> and phosphorus<sup>34,35</sup> into helicene frameworks, thereby expanding their electronic versatility and fine-tuning their photophysical profiles. For example, the incorporation of pyrrole-type nitrogen atoms into helicene backbone has been shown to substantially destabilize the HOMO level, resulting in a bathochromic shift of absorption and emission spectra, as well as an increase in fluorescence quantum yield when compared to their carbohelicenes counterparts.<sup>36–38</sup>

Simultaneously, molecular engineering has facilitated the integration of multiple helicene subunits into a single molecule.<sup>39</sup> These multi(hetero)helicenes not only display amplified chiroptical responses due to cooperative interactions among the helical units, but can also exist as stereoisomers with finely tunable optical behavior.<sup>40,41</sup> Recent progress has

<sup>a</sup> Institute of Organic Chemistry, Polish Academy of Sciences, Kasprzaka 44/52, 01-224 Warsaw, Poland. E-mail: dtgryko@icho.edu.pl

<sup>b</sup> Aix Marseille Univ, CNRS, Centrale Med, FSCM, Chiropole, Marseille, iSm2, Marseille, France

<sup>c</sup> Dipartimento di Chimica, Università degli Studi di Salerno, via Ponte don Melillo, 84084 Fisciano, SA, Italy. E-mail: gmonaco@unisa.it

<sup>d</sup> Department of Chemistry, Life Sciences and Environmental Sustainability, University of Parma, Parco Area delle Scienze 17/a, 43124 Parma, Italy.

E-mail: francesca.terenziani@unipr.it

<sup>e</sup> Faculty of Chemistry, University of Warsaw, Pasteura 1, 02-093 Warsaw, Poland. E-mail: mkc@chem.uw.edu.pl

<sup>f</sup> Inter-faculty Individual Studies in Mathematics and Natural Sciences, University of Warsaw, Stefana Banacha 2C, 02-097 Warsaw, Poland



been driven by strategies aimed at boosting CPL brightness ( $B_{\text{CPL}}$ ) as a key metric that integrates fluorescence quantum yield ( $\Phi_{\text{F}}$ ), molar absorption coefficient ( $\epsilon$ ), and luminescence dissymmetry factor ( $g_{\text{lum}}$ ), providing a comprehensive evaluation of CPL emitter performance.<sup>3</sup> This is particularly important given that relatively small helicenes typically exhibit low fluorescence quantum yields ( $\Phi_{\text{F}}$ )<sup>42,43</sup> and modest dissymmetry factors ( $g_{\text{lum}}$  and  $g_{\text{abs}}$ ).<sup>44</sup> Consequently, the rational design of multi(hetero)helicenes plays a critical role in enhancing these photophysical and chiroptical parameters.<sup>45</sup> For instance, lateral  $\pi$ -extension of the helicene backbone improves  $\Phi_{\text{F}}$  and  $\epsilon$ ,<sup>46–49</sup> while symmetric, delocalized architectures enhance  $g_{\text{lum}}$ ,<sup>50</sup> collectively guiding the rational design of high-performance CPL-active materials.

Despite these developments, much remains to be explored regarding multihelicene architectures based on unconventional cores. While traditional aromatic systems like benzene,<sup>51–59</sup> naphthalene<sup>60</sup> or pyrene<sup>61</sup> have been extensively utilized, more  $\pi$ -conjugated systems, such as perylene,<sup>62,63</sup> hexabenzocoronene<sup>64,65</sup> and corannulene,<sup>66–71</sup> allowed expanding the molecular design space to include more diverse and underrepresented scaffolds, which opens new avenues for innovation. Specifically, the incorporation of other than six-membered rings, often combined with heteroatom doping, such as nitrogen or boron, can significantly alter intramolecular strain, modulate aromaticity, and reshape molecular conformations of polycyclic helicenes.<sup>72–77</sup> These modifications not only fine-tune the chiroptical and photophysical properties but also affect the redox behavior, potentially leading to unprecedented electrochemical profiles.<sup>38,78</sup>

Previously, our group has reported several successful syntheses of helicenes featuring a 1,4-dihydropyrrolo[3,2-*b*]pyrrole (DHPP) core.<sup>79–81</sup> Notably, the most robust approach employed a double direct-arylation reaction as a straightforward and efficient synthetic strategy.<sup>82</sup> Building upon this foundation, we aimed to further exploit the highly electron-rich heteropentalene core by integrating multiple helical motifs, ultimately leading to the construction of a quadruple heterohelicene with a stable configuration and enhanced (chir)optical properties (Fig. 1).

## Results and discussion

### Design and synthesis

Building upon our previous results on direct arylation<sup>82</sup> and having in mind the electronic requirements for photocyclization reaction<sup>80</sup> as well as geometrical constraints of oxidative aromatic coupling (Scholl reaction) in the DHPP chemistry,<sup>81,83,84</sup> we designed a novel quadruple helicene composed of double anti-[S<sub>2</sub>]-type-[6]helicene embedding the central 1,4-dihydropyrrolo[3,2-*b*]pyrrole moiety and embedded in two [X]-type-[5]helicene units located on the periphery.<sup>85</sup>

We employed a general three-step protocol for the modular synthesis of nonplanar 1,4-dihydropyrrolo[3,2-*b*]pyrrole containing four aromatic subunits, starting from 2-(picen-13-yl)benzaldehyde (**1**), 4-octylaniline, and diacetyl (Scheme 1).<sup>86</sup>

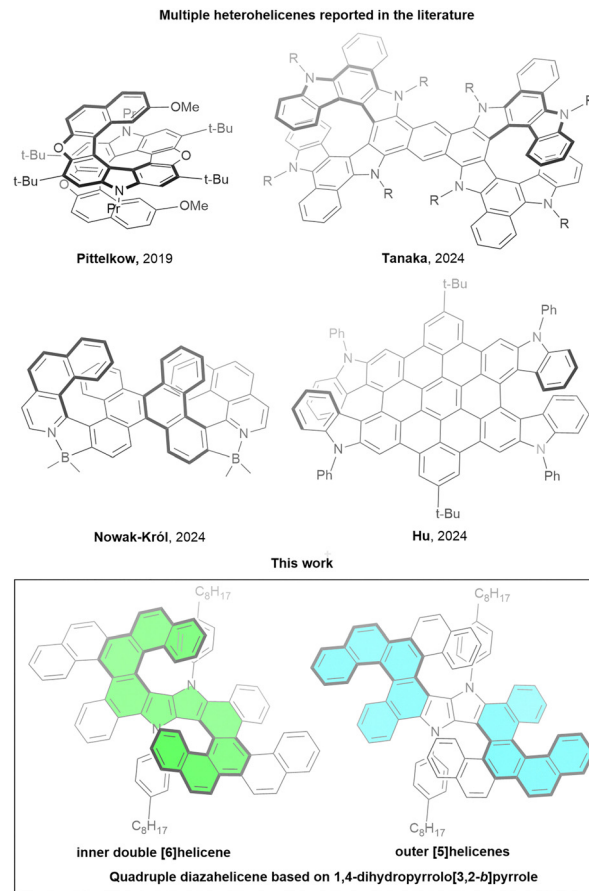


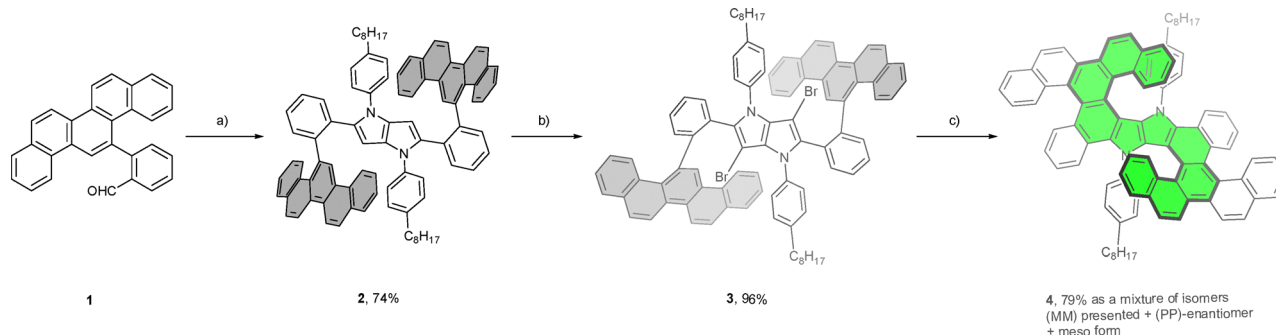
Fig. 1 Chemical structures of selected, previously reported aza-(multi)heterohelicenes.

The study commenced with the preparation of the respective aldehyde **1**. We utilized a Suzuki–Miyaura coupling using 2-formylphenylboronic acid and picen-13-yl triflate to obtain the *ortho*-aryl substituted benzaldehyde, while picen-13-ol was synthesized according to the reported one-pot pinacol-Ullmann procedure (see SI).<sup>87</sup>

With the aldehyde in hand, we readily prepared the tetra-arylpyrrolopyrrole **2** in a remarkable 74% yield by applying the optimized conditions developed by our group.<sup>86</sup> The compound **2** was subjected to a selective dibromination reaction of the DHPP core with NBS that yielded **3**, which was subsequently exposed to a two-fold Pd-catalyzed intramolecular direct arylation to smoothly produce the desired product as a mixture of isomers. In the transformation, two picene subunits are intramolecularly coupled to the pyrrolo[3,2-*b*]pyrrole core to produce two new rings, resulting in a quadruple diazahelicene.

The chosen route leverages on the recently published finding that 2-arylbenzaldehydes, which possess sterically demanding substituents in the *ortho* position (e.g. derivatives of naphthalene and fluorene) undergo a multicomponent reaction, providing respective TAPPs in exceptionally high yield.<sup>80,88</sup> It seems that their low solubility in the reaction mixture (toluene: acetic acid 1/1) pushes the equilibrium of the reaction towards their formation. Moreover, an important feature of our





**Scheme 1** Synthetic route to compound **4**. Reagents and conditions: (a) 4-*n*-octylaniline, butan-2,3-dione,  $\text{Fe}(\text{ClO}_4)_3 \cdot x\text{H}_2\text{O}$  (6% mol), AcOH/toluene, 50 °C, 16 h; (b) NBS,  $\text{CHCl}_3$ , reflux, overnight; (c)  $\text{Cs}_2\text{CO}_3$  (3 eq),  $\text{PPh}_3$  (0.5 eq),  $\text{Pd}(\text{OAc})_2$  (20% mol), toluene, 120 °C, overnight.

design is the utilization of *N*-aryl substituent on the pyrrolo[3,2-*b*]pyrrole core as a steric constraint for obtaining a stable configuration of the central double [6]helicene. The identity of the final compound was verified by variable temperature NMR analysis and high-resolution mass spectra, as well as by X-ray crystallography. In analogy to our recent study,<sup>80</sup> the helicene **4** exhibits temperature-dependent spectral features arising from the restricted rotation of the 4-octylbenzene substituents. At room temperature, the  $^1\text{H}$  NMR spectrum displays coalescence of the signals corresponding to the protons of the 4-octylbenzene units, indicating dynamic averaging. Upon cooling, broad signal around 6.5 ppm resolve into distinct peaks, confirming a slow exchange regime and highlighting the torsional restriction of the aryl groups (Fig. 2). This spectral clarity at lower temperatures supports the presence of conformational rigidity imposed by those substituents. The helicene **4** is stable under ambient light in air at room temperature, as well as exhibits good solubility in toluene and dichloromethane.

The helicene **4** was obtained as a mixture of diastereomers, consisting of a pair of enantiomers and a *meso*-form. Chiral HPLC separation allowed for the isolation of the stereoisomers in a pure state. The racemic fraction, which accounted for approximately 30% of the initial mixture subjected to separation, was resolved into its individual enantiomers in nearly equimolar ratio (1:1). Both enantiomers were successfully isolated with an enantiomeric excess (ee) of 99.5%, as determined by chiral HPLC. Further experimental details are provided in the SI.

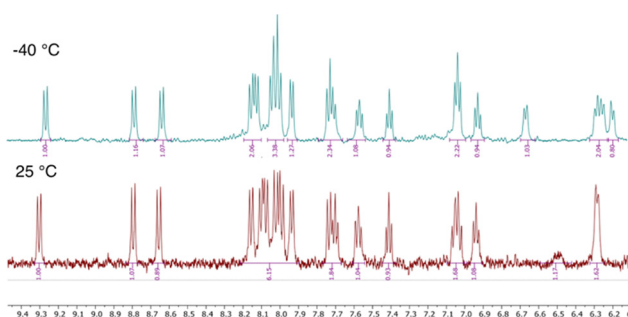


**Fig. 2** Variable temperature  $^1\text{H}$  NMR experiment. Comparison of aromatic signals for enantiomeric form of **4**.

### X-ray structure

The *meso*-form of the molecule **4** crystallizes in triclinic  $P\bar{1}$  space group with three halves forming the asymmetric part of the unit cell. These halves are located at inversion centers, so the unit cell consists of three molecules. They are highly distorted and form a helical structure, differing mainly in the disorder of the octyl substituents. The geometry of the helices is quite similar, although not identical (see Fig. 3 for the representative molecule), and their shape allows for an intramolecular  $\pi$ - $\pi$  interaction between the outer picene scaffold and the benzene ring. The distance between those rings varies from 3.08 Å to 3.20 Å, so the interactions are not strong. The DHPP core acting as a linker between benzenoid fragments is planar and does not participate in intramolecular interactions.

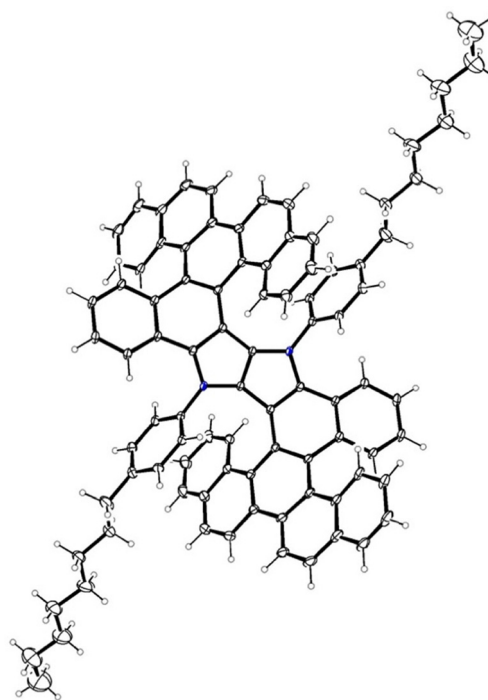


**Fig. 3** Molecule in the crystal of the *meso*-form of compound **4**. Crystal data: triclinic,  $P\bar{1}$ ,  $a = 15.5568(12)$ ,  $b = 20.3308(16)$ ,  $c = 20.5121(17)$  Å,  $\alpha = 101.392(3)$ ,  $\beta = 102.858(3)$ ,  $\gamma = 104.546(3)$ . The displacement ellipsoids are given at 30% probability level.



The crystal structure is stabilized by weak intramolecular van der Waals interactions. More details can be found in the SI.

### Photophysical properties

Steady-state absorption and emission spectra were recorded to probe the fundamental spectroscopic properties of dye **4** (Fig. 4 and 5). To evaluate the impact of the solvent on absorption and fluorescence spectra of both diastereoisomeric helicenes, spectroscopic measurements were performed in dichloromethane and toluene. All stereoisomers exhibited a prominent absorption band spanning from the high-energy UV region ( $\approx 300$  nm) to approximately 500 nm. Integration of the absorption peaks gives very high values of oscillator strengths ( $f > 1$ ), Fig. S16, S17 and Table S3, which, according to the DFT calculations presented later, can be only partly attributed to unresolved resonances. According to DFT calculations, the transitions within the absorption band can be attributed to  $\pi$ - $\pi^*$  transitions extending over all the conjugated pattern, with a character of charge transfer from the nitrogen towards other parts of the helicene (see later). Notably, the *meso*-form displayed higher molar absorption coefficients ( $\epsilon$ ) than the enantiomers in both solvents. Nevertheless, the molar extinction coefficient at  $\approx 475$  nm was approximately  $4700 \text{ M}^{-1} \text{ cm}^{-1}$  for all stereoisomers. In the emission spectra of all stereoisomers, vibronic features were largely smeared out by inhomogeneous broadening, with a stronger effect in the mildly polar DCM solvent than in the non-polar toluene.

### (Chir)optical properties

The CD spectra of the enantiomers of **4** in dichloromethane (Fig. 6) display multiple peaks, with absorption dissymmetry factors ( $g_{\text{abs}}$ ) remaining below  $10^{-2}$  (Fig. S14). CPL spectra were recorded by exciting the samples at 405 nm, with a horizontal polarizer placed in the excitation path to avoid potential artifacts arising from linearly polarized emission components.<sup>89</sup> The raw CPL data were smoothed using a Savitzky-Golay filter. As shown in Fig. 6, the CPL spectrum closely resembles the fluorescence

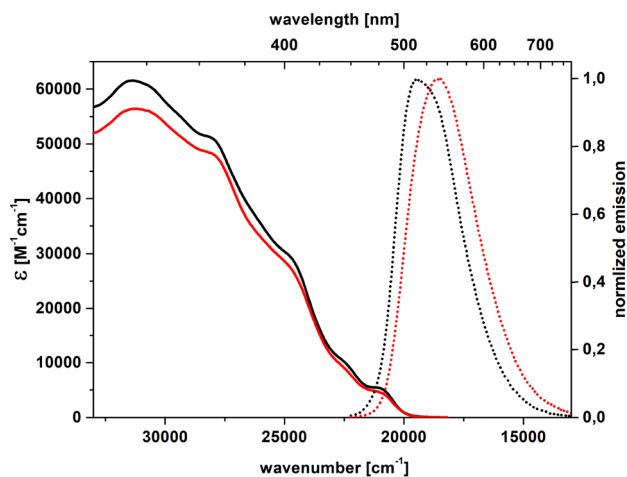


Fig. 4 Absorption (solid) and emission (dot) spectra of (*P,PP,P*)-enantiomer of **4** (black – toluene, red – dichloromethane).

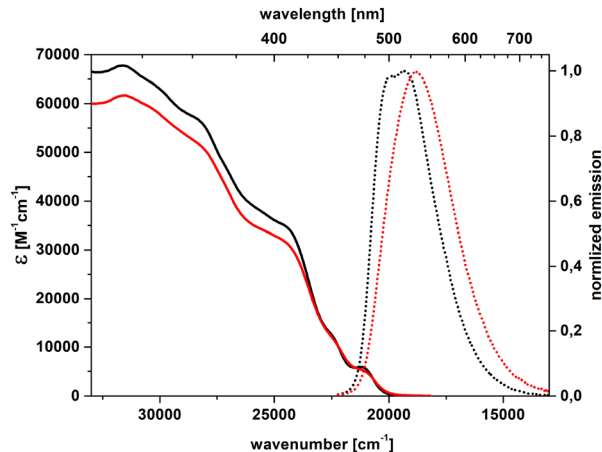


Fig. 5 Absorption (solid) and emission (dot) spectra of *meso*-form of dye **4** (black – toluene, red – dichloromethane).

spectrum recorded in the same solvent (Fig. 4). The dissymmetry factor for CPL ( $g_{\text{lum}}$ ) is approximately  $1.1 \times 10^{-3}$  (absolute value), suggesting moderate chiral luminescence activity. Notably,  $g_{\text{lum}}$  is lower than the  $g_{\text{abs}}$  value of the lowest-energy CD peak ( $3.9 \times 10^{-3}$ ), suggesting sizable structural rearrangements after excitation, prior to emission.

To further assess the chiroptical performance of **4**, its circularly polarized luminescence brightness ( $B_{\text{CPL}}$ ) was determined according to the expression:<sup>3</sup>

$$B_{\text{CPL}} = \frac{1}{2} g_{\text{lum}} \cdot \Phi_{\text{F}} \cdot \epsilon$$

where  $\Phi_{\text{F}}$  is the fluorescence quantum yield and  $\epsilon$  is the molar absorptivity at a fixed wavelength (usually the absorption maximum). The  $B_{\text{CPL}}$  calculated for helicene **4** in dichloromethane, for excitation at 320 nm, amounts to  $5.1 \text{ M}^{-1} \text{ cm}^{-1}$  (Table 1), classifying the compound as a moderate CPL emitter.<sup>4</sup>

Additional measurements were performed in toluene (Fig. S15), to address the effect of the solvent polarity. The  $|g_{\text{lum}}|$  factor amounts to  $1.8 \times 10^{-3}$ , sizably higher than the one obtained in dichloromethane: this, together with the higher

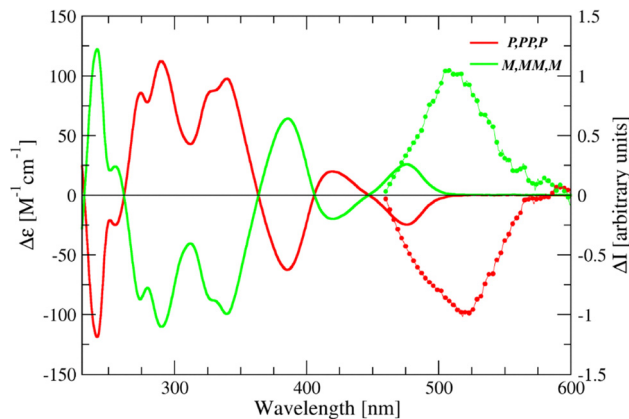


Fig. 6 CD (solid lines) and CPL (dotted lines) spectra of the two enantiomeric atropisomers PP and MM of **4** in dichloromethane.



**Table 1** CPL dissymmetry factor ( $g_{lum}$ ), fluorescence quantum yield, absorption coefficient at 320 nm and CPL brightness of the two enantiomeric atropisomers PP and MM of **4** in dichloromethane and toluene

Solvent	$g_{lum}$ ( <i>P,PP,P</i> / <i>M,MM,M</i> )	$\Phi_F$	$\epsilon_{320\text{ nm}}$ [ $M^{-1}\text{ cm}^{-1}$ ]	$B_{CPL}$ [ $M^{-1}\text{ cm}^{-1}$ ]
CH <sub>2</sub> Cl <sub>2</sub>	$-1.1 \times 10^{-3}/1.1 \times 10^{-3}$	0.16	58 000	5.1
Toluene	$-1.8 \times 10^{-3}/1.8 \times 10^{-3}$	0.20	65 000	11.7

fluorescence quantum yield, leads to a more than doubled  $B_{CPL}$  value, amounting to  $11.7\text{ M}^{-1}\text{ cm}^{-1}$  (Table 1).

### Computational studies

DFT computations have been carried out to determine the absolute configuration of the two eluted fractions (see SI for details). The geometry of the quadruple helicenes can be described in terms of the *P* or *M* helicity of the four helicene units: the two lateral [5]helicenes and two central abutting [5]aza-helicenes. Despite the ease of isomerization of [5]helicenes,<sup>90</sup> the central fragments do contribute to stable chirality at room temperature, thanks to the benzene ring linked with the nitrogen atom. Therefore, we expect 3 atropisomers, each having 4 conformers, e.g. for the stable configuration *PP* of the two central helicenes, at room temperature we expect the thermal average of the four rapidly interconverting configurations *P,PP,P*, *M,PP,P*, *P,PP,M* and *M,PP,M*. Calculated conformational free energies at the BP86-D3/TZVP-PCM level (see Tables S4 and S5) show that the configuration of each lateral helicene is mainly induced by the central helicene, so that the dominating conformations are the  $C_2$  enantiomers (*P,PP,P*) and (*M,MM,M*) and the  $C_1$  meso-form (*M,MP,P*). According to the calculations, thermodynamic equilibrium in DCM at room temperature would lead to 12% of racemic form, which is in qualitative agreement with the 30% stereoselectivity of the reaction. The presence of more than a single conformer at room temperature is clearly appreciated from the temperature change of the NMR spectrum (Fig. 2); according to calculations (see Table S6) the H atoms undergoing significant changes with temperature are those of the 4-alkylbenzene substituents, as well as some H attached to the lateral [5]helicenes. Therefore, the simulation of the ECD spectra at room temperature, has been performed first considering the thermal average of the spectra of the conformers. The simulation of the ECD spectrum as sum of Gaussians with frequencies and intensities taken from the TD-DFT computation, after a constant blue-shift of all the resonance frequencies and multiplication of all computed intensities by a scale factor, indicate that *PP* atropisomer, i.e. the thermal average of the 4 *PP*-centered conformers, leads to the best match with the ECD spectrum of the first eluted fraction (Fig. 7). The same result is obtained considering only the best matching conformer of the two atropisomers. Quantitative analysis of the computed and experimental spectra in terms of the cosine similarity (COSI),<sup>91,92</sup> which is a robust goodness-of-fit indicator, together with the errors associated with it,<sup>93</sup> fully confirms the better ability of the *PP* atropisomer

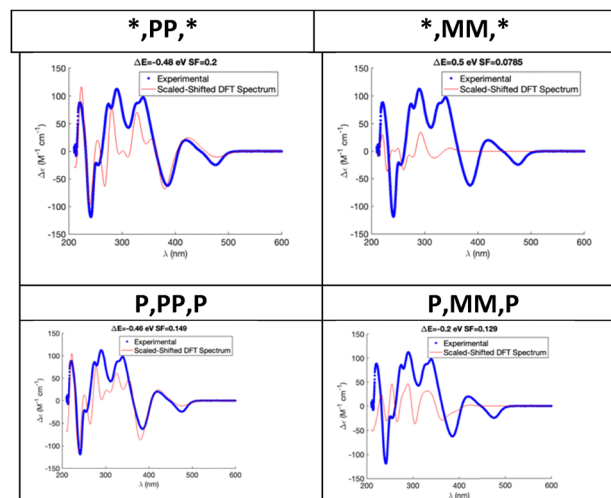


**Fig. 7** Comparison of experimental and DFT spectra for the studied azahelicene. Calculations have been performed at the wB97X-D/TZVP-PCM//BP86-D3/TZVP-PCM level. Gaussian functions with HWFM of 0.25 eV have been used to generate the computed spectra. The two top figures are the free-energy weighted spectra of the 4 conformers of each atropisomer (the symbol \* stands for the thermal average over *P* and *S* helicity of the lateral [5]helicenes). The two bottom figures show the comparison for the more abundant conformers of the two atropisomers.

to reproduce the ECD trace of the first eluted fraction (see Table S7 and the SI for details).

An independent confirmation of the absolute configuration of the first eluted fraction comes from its negative  $g_{lum}$ , and the values computed for the *P,PP,P* conformer which are of the same sign, although overestimated in magnitude ( $-3.7 \times 10^{-3}$  in dichloromethane and  $-3.6 \times 10^{-3}$  in toluene).

The TD-DFT calculations provide information on the nature of the excited states, which, due to the  $C_2$  symmetry can be labelled as A and B. Symmetric states (A) can couple with the symmetric ground state only through the *z* component of the electric or the magnetic dipole. In pristine helicenes, the unique symmetry axis is perpendicular to the helical axis, and, consistently, considering that the molecules extend perpendicularly to the symmetry axis, transitions with larger oscillator strength are from the ground state A to B states.<sup>94</sup> In our molecule the *z* axis is not strictly perpendicular to any of the axes of the four helical fragments, but the molecule still develops mainly perpendicularly to the *z* axis. Indeed, larger dipole-allowed transitions are still of B symmetry (Table S8). In particular, the first excited energy of B symmetry is already stronger than the second of A symmetry, so that the strategy of a synthesis-driven orbital permutation for the enhancement of luminescence<sup>95</sup> cannot be pursued in this case. The lowest energy excited state (mainly of HOMO → LUMO character), as well as that with the strongest absorption (state 7, mainly of HOMO-1 → LUMO+2 character), are endowed of a charge transfer from the DHPP core towards the helicenes, as can be inferred from the sketches of the orbitals (Fig. S19). Consistently, the first excited state can be expected to have an enhanced dipole. Indeed we computed an increase of dipole



passing from the ground to the first excited state: from 0.6925 to 1.0872 D (in DCM) and from 0.9021 D to 1.1734 D (in toluene). The increased dipole in the excited state is consistent with the solvatochromic effect reported above.

## Conclusions

We have demonstrated that easily available 1,2,4,5-tetraarylpyrrolo[3,2-*b*]pyrroles constitute a perfect core for building nonplanar aromatic systems. The methodology is general and makes it possible to incorporate multiple helicities to make S-shaped helicenes in only three steps. The enantiomers of quadruple helicene based on a DHPP core were resolved by semipreparative HPLC to afford enantiomerically pure samples. Photophysical and chiroptical properties of purified stereoisomers were studied by UV-Vis and ECD spectra. The findings highlight the importance of a combination of electron-rich heterocycles like 1,4-dihydropyrrolo[3,2-*b*]pyrroles with multiple helicities to enhance chiroptical behavior. By elucidating the relationship between molecular structure and chiroptical activity, this work provides valuable insights for the rational design of next-generation chiral materials.

## Author contributions

Conceptualization: K. G., D. T. G.; investigation: K. J. K., A. C., F. B., A. L., N. V.; supervision: D. T. G., F. T., M. K. C., G. M., D. K., K. G.; visualization: K. J. K., A. C., F. B., A. L., N. V.; writing – original draft: K. J. K., D. T. G., F. T., M. K. C., G. M., D. K., K. G.; writing – review & editing: K. J. K., D. T. G., F. T., G. M., K. G.

## Conflicts of interest

There are no conflicts to declare.

## Data availability

The data underlying this study are available in the published article and its Supporting Information. Experimental procedures, X-ray crystallography data, photophysical properties, computational studies and copies of the NMR spectra of all products (PDF). Supplementary information: detailed synthetic protocols, characterization data;  $^1\text{H}$ ,  $^{13}\text{C}\{^1\text{H}\}$  NMR and HRMS spectra, computational details and analyses, photophysical measurement results, CD and CPL spectra, chiral HPLC separation data, optical rotation values, crystal structure and additional figures as cited in the main text. See DOI: <https://doi.org/10.1039/d5tc04545b>.

CCDC 2494310 contains the supplementary crystallographic data for this paper.<sup>96</sup>

## Acknowledgements

This work has received funding from the European Union's Horizon 2020 research and innovation programme under the

Marie Skłodowska-Curie grant agreements no. 101007804 (Micro4Nano) and no. 860762. The work was financially supported by the Polish National Science Centre, Poland (OPUS 2020/37/B/ST4/00017) and has benefited from the equipment and framework of the COMP-HUB and COMP-R initiatives, funded by the “Departments of Excellence” program of the Italian Ministry for University and Research (MIUR, 2018–2022 and MUR, 2023–2027). G. M. and A. L. acknowledge financial support from MUR. Assistance of prof. Ilona Turowska-Tyrk (University of Warsaw) in final modelling disorder of the structure is highly appreciated.

## Notes and references

- 1 Y. Shen and C.-F. Chen, *Chem. Rev.*, 2012, **112**, 1463–1535.
- 2 N. Berova, L. D. Bari and G. Pescitelli, *Chem. Soc. Rev.*, 2007, **36**, 914.
- 3 L. Arrico, L. Di Bari and F. Zinna, *Chem. – Eur. J.*, 2021, **27**, 2920–2934.
- 4 M. Cei, L. Di Bari and F. Zinna, *Chirality*, 2023, **35**, 192–210.
- 5 J. L. Greenfield, J. Wade, J. R. Brandt, X. Shi, T. J. Penfold and M. J. Fuchter, *Chem. Sci.*, 2021, **12**, 8589–8602.
- 6 J. Meisenheimer and K. Witte, *Ber. Dtsch. Chem. Ges.*, 1903, **36**, 4153–4164.
- 7 S. Jhulki, A. K. Mishra, T. J. Chow and J. N. Moorthy, *Chem. – Eur. J.*, 2016, **22**, 9375–9386.
- 8 K. Dhbaibi, L. Abella, S. Meunier-Della-Gatta, T. Roisnel, N. Vanthuyne, B. Jamoussi, G. Pieters, B. Racine, E. Quesnel, J. Autschbach, J. Crassous and L. Favereau, *Chem. Sci.*, 2021, **12**, 5522–5533.
- 9 Y. Yang, R. C. Da Costa, M. J. Fuchter and A. J. Campbell, *Nat. Photonics*, 2013, **7**, 634–638.
- 10 P. Josse, L. Favereau, C. Shen, S. Dabos-Seignon, P. Blanchard, C. Cabanetos and J. Crassous, *Chem. – Eur. J.*, 2017, **23**, 6277–6281.
- 11 J. M. Dos Santos, D. Sun, J. M. Moreno-Naranjo, D. Hall, F. Zinna, S. T. J. Ryan, W. Shi, T. Matulaitis, D. B. Cordes, A. M. Z. Slawin, D. Beljonne, S. L. Warriner, Y. Olivier, M. J. Fuchter and E. Zysman-Colman, *J. Mater. Chem. C*, 2022, **10**, 4861–4870.
- 12 M. Hasan, V. N. Khose, T. Mori, V. Borovkov and A. V. Karnik, *ACS Omega*, 2017, **2**, 592–598.
- 13 P. Aillard, A. Voituriez and A. Marinetti, *Dalton Trans.*, 2014, **43**, 15263–15278.
- 14 W.-L. Zhao, M. Li, H.-Y. Lu and C.-F. Chen, *Chem. Commun.*, 2019, **55**, 13793–13803.
- 15 A. V. Gulevskaya, E. A. Shvydkova and D. I. Tonkoglavova, *Eur. J. Org. Chem.*, 2018, 5030–5043.
- 16 Y. Matsuo, M. Gon, K. Tanaka, S. Seki and T. Tanaka, *J. Am. Chem. Soc.*, 2024, **146**, 17428–17437.
- 17 T. Kawashima, Y. Matsumoto, T. Sato, Y. M. A. Yamada, C. Kono, A. Tsurusaki and K. Kamikawa, *Chem. – Eur. J.*, 2020, **26**, 13170–13176.
- 18 F. Ammon, S. T. Sauer, R. Lippert, D. Lungerich, D. Reger, F. Hampel and N. Jux, *Org. Chem. Front.*, 2017, **4**, 861–870.



- 19 C. Dusold, D. I. Sharapa, F. Hampel and A. Hirsch, *Chem. – Eur. J.*, 2021, **27**, 2332–2341.
- 20 Y. Matsuo, M. Gon, K. Tanaka, S. Seki and T. Tanaka, *Chem. – Asian J.*, 2024, **19**, e202400134.
- 21 J. Borstelmann, S. Zank, M. Krug, G. Berger, N. Fröhlich, G. Glotz, F. Gnannt, L. Schneider, F. Rominger, F. Deschler, T. Clark, G. Gescheidt, D. M. Guldi and M. Kivala, *Angew. Chem., Int. Ed.*, 2025, e202423516.
- 22 X. Tian, K. Shoyama, B. Mahlmeister, F. Brust, M. Stolte and F. Würthner, *J. Am. Chem. Soc.*, 2023, **145**, 9886–9894.
- 23 J. Liu, J. Hong, Z. Liao, J. Tan, H. Liu, E. Dmitrieva, L. Zhou, J. Ren, X. Cao, A. A. Popov, Y. Zou, A. Narita and Y. Hu, *Angew. Chem., Int. Ed.*, 2024, **63**, e202400172.
- 24 A. Nowak-Król, P. T. Geppert and K. R. Naveen, *Chem. Sci.*, 2024, **15**, 7408–7440.
- 25 F. Full, A. Artigas, K. Wiegand, D. Volland, K. Szkodzińska, Y. Coquerel and A. Nowak-Król, *J. Am. Chem. Soc.*, 2024, **146**, 29245–29254.
- 26 J. Full, M. J. Wildervanck, C. Dillmann, S. P. Panchal, D. Volland, F. Full, K. Meerholz and A. Nowak-Król, *Chem. – Eur. J.*, 2023, **29**, e202302808.
- 27 D. Volland, J. Niedens, P. T. Geppert, M. J. Wildervanck, F. Full and A. Nowak-Król, *Angew. Chem., Int. Ed.*, 2023, **62**, e202304291.
- 28 T. Katayama, S. Nakatsuka, H. Hirai, N. Yasuda, J. Kumar, T. Kawai and T. Hatakeyama, *J. Am. Chem. Soc.*, 2016, **138**, 5210–5213.
- 29 M. Schnitzlein, K. Shoyama and F. Würthner, *Chem. Sci.*, 2024, **15**, 2984–2989.
- 30 J.-K. Li, X.-Y. Chen, Y.-L. Guo, X.-C. Wang, A. C.-H. Sue, X.-Y. Cao and X.-Y. Wang, *J. Am. Chem. Soc.*, 2021, **143**, 17958–17963.
- 31 F. Zhou, Z. Huang, Z. Huang, R. Cheng, Y. Yang and J. You, *Org. Lett.*, 2021, **23**, 4559–4563.
- 32 W. Yang, Z. Ren, J. Feng, Z. Lv, X. Cheng, J. Zhang, D. Du, C. Chi and J. Shen, *Angew. Chem.*, 2024, **136**, e202412681.
- 33 Y. Ma, L. Zhou, J. Tan, W. Sun, Y. Zou and Y. Hu, *Adv. Opt. Mater.*, 2025, **13**, 2402446.
- 34 B. Yang, S. Yan, C. Li, H. Ma, F. Feng, Y. Zhang and W. Huang, *Chem. Sci.*, 2023, **14**, 10446–10457.
- 35 K. Yavari, W. Delaunay, N. De Rycke, T. Reynaldo, P. Aillard, M. Srebro-Hooper, V. Y. Chang, G. Muller, D. Tondelier, B. Geffroy, A. Voituriez, A. Marinetti, M. Hissler and J. Crassous, *Chem. – Eur. J.*, 2019, **25**, 5303–5310.
- 36 X. Guo, Z. Yuan, Y. Zhu, Z. Li, R. Huang, Z. Xia, W. Zhang, Y. Li and J. Wang, *Angew. Chem.*, 2019, **131**, 17122–17128.
- 37 D. Reger, P. Haines, K. Y. Amsharov, J. A. Schmidt, T. Ullrich, S. Bönisch, F. Hampel, A. Görling, J. Nelson, K. E. Jelfs, D. M. Guldi and N. Jux, *Angew. Chem., Int. Ed.*, 2021, **60**, 18073–18081.
- 38 S. S. Warthegau, A. E. Hillers-Bendtsen, S. K. Pedersen, C. Rindom, C. Bræstrup, J. S. Jensen, O. Hammerich, M. S. Thomsen, F. S. Kamounah, P. Norman, K. V. Mikkelsen, T. Brock-Nannestad and M. Pittelkow, *Chem. – Eur. J.*, 2023, **29**, e202301815.
- 39 A. Tsurusaki and K. Kamikawa, *Chem. Lett.*, 2021, **50**, 1913–1932.
- 40 C. Li, Y. Yang and Q. Miao, *Chem. – Asian J.*, 2018, **13**, 884–894.
- 41 K. Kato, Y. Segawa and K. Itami, *Synlett*, 2019, 370–377.
- 42 M. Sapir and E. V. Donckt, *Chem. Phys. Lett.*, 1975, **36**, 108–110.
- 43 J. B. Birks, D. J. S. Birch, E. Cordemans and E. Vander Donckt, *Chem. Phys. Lett.*, 1976, **43**, 33–36.
- 44 H. Tanaka, Y. Inoue and T. Mori, *ChemPhotoChem*, 2018, **2**, 386–402.
- 45 H. Tanaka, Y. Kato, M. Fujiki, Y. Inoue and T. Mori, *J. Phys. Chem. A*, 2018, **122**, 7378–7384.
- 46 Y. Shen, N. Yao, L. Diao, Y. Yang, X. Chen and H. Gong, *Angew. Chem., Int. Ed.*, 2023, **62**, e202300840.
- 47 Z. Qiu, C.-W. Ju, L. Frédéric, Y. Hu, D. Schollmeyer, G. Pieters, K. Müllen and A. Narita, *J. Am. Chem. Soc.*, 2021, **143**, 4661–4667.
- 48 C. M. Cruz, S. Castro-Fernández, E. Maçôas, J. M. Cuerva and A. G. Campaña, *Angew. Chem., Int. Ed.*, 2018, **57**, 14782–14786.
- 49 V. Kumar, J. L. Páez, S. Míguez-Lago, J. M. Cuerva, C. M. Cruz and A. G. Campaña, *Chem. Soc. Rev.*, 2025, **54**, 4922–4947.
- 50 H. Tanaka, M. Ikenosako, Y. Kato, M. Fujiki, Y. Inoue and T. Mori, *Commun. Chem.*, 2018, **1**, 38.
- 51 J. Luo, X. Xu, R. Mao and Q. Miao, *J. Am. Chem. Soc.*, 2012, **134**, 13796–13803.
- 52 L. Barnett, D. M. Ho, K. K. Baldrige and R. A. Pascal, *J. Am. Chem. Soc.*, 1999, **121**, 727–733.
- 53 A. Pradhan, P. Dechambenoit, H. Bock and F. Durola, *Angew. Chem., Int. Ed.*, 2011, **50**, 12582–12585.
- 54 H. Saito, A. Uchida and S. Watanabe, *J. Org. Chem.*, 2017, **82**, 5663–5668.
- 55 T. Hosokawa, Y. Takahashi, T. Matsushima, S. Watanabe, S. Kikkawa, I. Azumaya, A. Tsurusaki and K. Kamikawa, *J. Am. Chem. Soc.*, 2017, **139**, 18512–18521.
- 56 V. Bereznaia, M. Roy, N. Vanthuyne, M. Villa, J.-V. Naubron, J. Rodriguez, Y. Coquerel and M. Gingras, *J. Am. Chem. Soc.*, 2017, **139**, 18508–18511.
- 57 M. Roy, V. Bereznaia, M. Villa, N. Vanthuyne, M. Giorgi, J. Naubron, S. Poyer, V. Monnier, L. Charles, Y. Carissan, D. Hagebaum-Reignier, J. Rodriguez, M. Gingras and Y. Coquerel, *Angew. Chem., Int. Ed.*, 2020, **59**, 3264–3271.
- 58 F. Zhang, E. Michail, F. Saal, A. Krause and P. Ravat, *Chem. – Eur. J.*, 2019, **25**, 16241–16245.
- 59 A. Artigas, F. Rigoulet, M. Giorgi, D. Hagebaum-Reignier, Y. Carissan and Y. Coquerel, *J. Am. Chem. Soc.*, 2023, **145**, 15084–15087.
- 60 T. Fujikawa, Y. Segawa and K. Itami, *J. Am. Chem. Soc.*, 2015, **137**, 7763–7768.
- 61 C. Wallerius, O. Erdene-Ochir, E. V. Doeselar, R. Alle, A. T. Nguyen, M. F. Schumacher, A. Lützen, K. Meerholz and S. H. Pun, *Precis. Chem.*, 2024, **2**, 488–494.
- 62 S. H. Pun, K. M. Cheung, D. Yang, H. Chen, Y. Wang, S. V. Kershaw and Q. Miao, *Angew. Chem.*, 2022, **134**, e202113203.
- 63 J. Li, X. Chen, W. Zhao, Y. Guo, Y. Zhang, X. Wang, A. C. H. Sue, X. Cao, M. Li, C. Chen and X. Wang, *Angew. Chem.*, 2023, **135**, e202215367.



- 64 Y. Zhu, Z. Xia, Z. Cai, Z. Yuan, N. Jiang, T. Li, Y. Wang, X. Guo, Z. Li, S. Ma, D. Zhong, Y. Li and J. Wang, *J. Am. Chem. Soc.*, 2018, **140**, 4222–4226.
- 65 Y. Wang, Z. Yin, Y. Zhu, J. Gu, Y. Li and J. Wang, *Angew. Chem., Int. Ed.*, 2019, **58**, 587–591.
- 66 K. Kato, Y. Segawa, L. T. Scott and K. Itami, *Angew. Chem., Int. Ed.*, 2018, **57**, 1337–1341.
- 67 H.-A. Lin, K. Kato, Y. Segawa, L. T. Scott and K. Itami, *Chem. Sci.*, 2019, **10**, 2326–2330.
- 68 K. Kise, S. Ooi, H. Saito, H. Yorimitsu, A. Osuka and T. Tanaka, *Angew. Chem., Int. Ed.*, 2022, **61**, e202112589.
- 69 D. Meng, G. Liu, C. Xiao, Y. Shi, L. Zhang, L. Jiang, K. K. Baldridge, Y. Li, J. S. Siegel and Z. Wang, *J. Am. Chem. Soc.*, 2019, **141**, 5402–5408.
- 70 Y. Wu, S. Ying, S. Liao, L. Zhang, J. Du, B. Chen, H. Tian, F. Xie, H. Xu, S. Deng, Q. Zhang, S. Xie and L. Zheng, *Angew. Chem., Int. Ed.*, 2022, **61**, e202204334.
- 71 Y.-F. Wu, S.-W. Ying, L.-Y. Su, J.-J. Du, L. Zhang, B.-W. Chen, H.-R. Tian, H. Xu, M.-L. Zhang, X. Yan, Q. Zhang, S.-Y. Xie and L.-S. Zheng, *J. Am. Chem. Soc.*, 2022, **144**, 10736–10742.
- 72 J. Wang, H. Shi, N. Xu, J. Zhang, Y. Yuan, M. Lei, L. Wang and P. Wang, *Adv. Funct. Mater.*, 2020, **30**, 2002114.
- 73 S. Qiu, A. C. Valdivia, W. Zhuang, F.-F. Hung, C.-M. Che, J. Casado and J. Liu, *J. Am. Chem. Soc.*, 2024, **146**, 16161–16172.
- 74 Z. Qiu, S. Asako, Y. Hu, C.-W. Ju, T. Liu, L. Rondin, D. Schollmeyer, J.-S. Lauret, K. Müllen and A. Narita, *J. Am. Chem. Soc.*, 2020, **142**, 14814–14819.
- 75 X.-L. Chen, S.-Q. Yu, Z.-Y. Cheng, Z.-Y. Zheng, A.-N. Chen, J. Bai, J.-Q. Liang, C. Zheng, X. Huang and H.-Y. Gong, *Org. Lett.*, 2025, acs.orglett.5c00294.
- 76 K. Kawai, K. Kato, L. Peng, Y. Segawa, L. T. Scott and K. Itami, *Org. Lett.*, 2018, **20**, 1932–1935.
- 77 F. Gan, G. Zhang, J. Liang, C. Shen and H. Qiu, *Angew. Chem.*, 2024, **136**, e202320076.
- 78 C. Li, C. Zhang, P. Li, Y. Jia, J. Duan, M. Liu, N. Zhang and P. Chen, *Angew. Chem.*, 2023, **135**, e202302019.
- 79 W. D. Petrykowski, N. Vanthuyne, C. Naim, F. Bertocchi, Y. M. Poronik, A. Ciesielski, M. K. Cyrański, F. Terenziani, D. Jacquemin and D. T. Gryko, *Chem. Sci.*, 2025, **16**, 8338–8345.
- 80 D. Kusy, K. Górski, F. Bertocchi, M. Galli, N. Vanthuyne, F. Terenziani and D. T. Gryko, *Chem. – Eur. J.*, 2025, **31**, e202404632.
- 81 M. Krzeszewski, T. Kodama, E. M. Espinoza, V. I. Vullev, T. Kubo and D. T. Gryko, *Chem. – Eur. J.*, 2016, **22**, 16478–16488.
- 82 D. T. Gryko, D. Kusy, K. Górski, D. Jacquemin, F. Terenziani, F. Bertocchi, N. Vanthuyne, K. Noworyta, B. Szymański and R. Kamiński, *ChemRxiv*, 2025, preprint, DOI: [10.26434/chemrxiv-2025-jp978](https://doi.org/10.26434/chemrxiv-2025-jp978).
- 83 M. Krzeszewski, K. Sahara, Y. M. Poronik, T. Kubo and D. T. Gryko, *Org. Lett.*, 2018, **20**, 1517–1520.
- 84 M. Krzeszewski, P. Świder, Ł. Dobrzycki, M. K. Cyrański, W. Danikiewicz and D. T. Gryko, *Chem. Commun.*, 2016, **52**, 11539–11542.
- 85 T. Mori, *Chem. Rev.*, 2021, **121**, 2373–2412.
- 86 M. Tasiór, O. Vakuliuk, D. Koga, B. Koszarna, K. Górski, M. Grzybowski, Ł. Kielesiński, M. Krzeszewski and D. T. Gryko, *J. Org. Chem.*, 2020, **85**, 13529–13543.
- 87 S. Lin and T. You, *Tetrahedron*, 2008, **64**, 9906–9910.
- 88 K. Górski, L. Pejov, K. B. Jørgensen, I. Knysh, D. Jacquemin and D. T. Gryko, *Chem. – Eur. J.*, 2025, **31**, e202404094.
- 89 G. Longhi, E. Castiglioni, J. Koshoubu, G. Mazzeo and S. Abbate, *Chirality*, 2016, **28**, 696–707.
- 90 J. Barroso, J. L. Cabellos, S. Pan, F. Murillo, X. Zarate, M. A. Fernandez-Herrera and G. Merino, *Chem. Commun.*, 2018, **54**, 188–191.
- 91 A. Singhal, *IEEE Data Eng. Bull.*, 2001, **24**, 35–43.
- 92 G. Monaco, F. Aquino and R. Zanasi, *Phys. Chem. Chem. Phys.*, 2017, **19**, 28028–28036.
- 93 G. Monaco, G. Procida, A. Di Mola, W. Herrebout and A. Massa, *Chem. Phys. Lett.*, 2020, **739**, 137000.
- 94 F. Furche, R. Ahlrichs, C. Wachsmann, E. Weber, A. Sobanski, F. Vögtle and S. Grimme, *J. Am. Chem. Soc.*, 2000, **122**, 1717–1724.
- 95 H. Kubo, T. Hirose, T. Nakashima, T. Kawai, J. Hasegawa and K. Matsuda, *J. Phys. Chem. Lett.*, 2021, **12**, 686–695.
- 96 CCDC 2494310: Experimental Crystal Structure Determination, 2026, DOI: [10.5517/ccdc.csd.cc2pqjml](https://doi.org/10.5517/ccdc.csd.cc2pqjml).

